Applied Catalysis B: Environment and Energy 357 (2024) 124278

Contents lists available at ScienceDirect

Applied Catalysis B: Environment and Energy

journal homepage: www.elsevier.com/locate/apcatb

Tailored copper-based cathode design advances economic viability of electrocatalytic nitrate treatment with ammonia recovery in a scalable flow reactor

Chenxu Yan [a,b], Kuan-Lin Lee [a], Jacob P. Troutman [a,c], Carolyn E. Brady [c], Simon M. Humphrey [c], David M. Cwiertny [d,e], Syed Mubeen [e], Charles J. Werth [a,*]

[a] Department of Civil, Architectural and Environmental Engineering, The University of Texas at Austin, 301 E. Dean Keeton St, Stop C1786, Austin, TX 78712, United States
[b] Carollo Engineers, Inc., 10900 Stonelake Blvd, Building 2, Suite 126, Austin, TX 78759, United States
[c] Department of Chemistry, The University of Texas at Austin, 100 E. 24th St, Stop A1590, Austin, TX 78712, United States
[d] Department of Civil and Environmental Engineering, 4105 Seamans Center for the Engineering Arts and Sciences, The University of Iowa, Iowa City, IA 52242, United States
[e] Department of Chemical and Biochemical Engineering, 4133 Seamans Center for the Engineering Arts and Sciences, The University of Iowa, Iowa City, IA 52242, United States

ARTICLE INFO

Keywords:
Electrocatalytic reduction
Nitrate reduction
Copper
Indium
Cost comparison

ABSTRACT

Electrocatalytic reduction is a promising alternative to remove nitrate (NO_3^-) from water and potentially recover value-added ammonia, but advancements are needed to reduce costs and promote technology adoption. Five monometallic catalysts on activated carbon cloth (ACC) electrodes were evaluated for electrocatalytic NO_3^- treatment in a previously developed scalable flow reactor. We report Cu and, for the first time, In (as In_2O_3) are the best performing catalysts regarding NO_3^- reduction activity (0.45–2.4 L g_{metal}^{-1} min^{-1}), Faradaic efficiency (FE), and NH_4^+ selectivity, with intermediate NO_2^- accumulation using Cu and NH_2OH using In. We discovered trace Pd addition (i.e., 0.01 wt%) to Cu eliminates NO_2^- accumulation, while approximately doubling activity, and boosting FE and NH_4^+ selectivity (99 %). Activity of Cu–Pd/ACC decreased with repeated treatment cycles but was easily recovered *in situ* via electrochemical regeneration. Electrocatalytic NO_3^- reduction costs with the Cu–Pd electrode were estimated less than IX or catalytic treatment, indicating economic viability.

1. Introduction

Due to its widespread occurrence in natural waters [1–4] and health effects [5], NO_3^- was among the first contaminants regulated by the U.S. Environmental Protection Agency (EPA) [6] after the Safe Drinking Water Act was passed in 1974. A number of technologies have evolved to remove NO_3^- from water [7]. The most common is ion exchange (IX), followed by reverse osmosis (RO). Neither destroy NO_3^- but transfer it from one phase to another that still requires treatment and disposal [7]. Further, RO is relatively energy intensive and is typically only considered when concominant salt removal is required [7,8]. Another alternative is biological treatment, but it suffers from slow start-up times, sensitivity to influent water quality conditions, and concerns for pathogen growth in drinking water [7]. A promising alternative is electrocatalytic reduction of nitrate in the presence of a catalyst to enhance reaction kinetics and control end-product selectivity. This approach results in complete destruction of nitrate, with little to no start-up period and little concerns for promoting pathogen growth. However, concerns persist regarding this technology's reliability, control for end-product selectivity, and cost.

Electrocatalytic reduction relies on an applied current to supply electrons for NO_3^- reduction, either directly or via conversion of protons to atomic hydrogen. It emerged as a more promising alternative than conventional catalytic treatment, which requires H_2 gas addition as the electron donor. H_2 gas represents a safety concern during storage and handling, and results in gas-liquid mass transfer limitations in the fixed-bed reactors likely required at water treatment plants [9,10]. Early studies of electrocatalytic NO_3^- reduction used pure metal(s) or metal particles deposited on conductive supports as the working electrode. The most studied metal particles are platinum group metals (PGMs)

* Corresponding author.
E-mail address: werth@utexas.edu (C.J. Werth).

https://doi.org/10.1016/j.apcatb.2024.124278
Received 31 August 2023; Received in revised form 4 June 2024; Accepted 6 June 2024
Available online 7 June 2024
0926-3373/Published by Elsevier B.V.

including Pd [11–13], Pt [14–16], Rh [17–19], Ir [20], and Ru [21], followed by the coinage metal Cu [22,23], and in a few instances, Sn [24,25]. In some cases, these metals were combined with one another to form bimetallic catalysts [26,27]. Common supports include activated carbon cloth, carbon paper, and glassy carbon electrodes.

The aforementioned choice of metals is partially supported by an experimental survey that used a suite of pure metal foils as working electrodes for NO_3^- reduction [21]. They determined relative activities (i.e., current density) of PGMs are Rh>Ru>Ir>Pd∼Pt, and those of coinage metals are Cu>Ag>Au. The choice of these metals is also partially supported by a more recent density functional theory (DFT) study that calculated NO_3^- reduction activities for different metals at 0 V/RHE [28], the thermodynamic potential at the onset of the hydrogen evolution reaction (HER). At and above this potential, HER is minimized such that the applied current is primarily directed toward NO_3^- reduction resulting in a greater Faradaic efficiency. The results indicate that the most active metals at this potential are Ru, Ir, Cu, and Co, but not Rh, Pd, Pt, Ag, or Au.

Lacking is experimental data elucidating how the most promising metals evaluated as pure foils or via DFT perform on realistic electrode supports in a scalable electrocatalytic reactor, including their relative NO_3^- reduction activity, selectivity for either dinitrogen or ammonia, and overall energy consumption. Ammonia is usually the dominant end product during electrocatalytic nitrate reduction, and its recovery is touted as a way to offset production via the energy intensive Haber-Bosch process [29]. However, nitrate reduction can stall at one or more intermediates, and dinitrogen production can be a preferred end product for direct drinking water treatment. Overall energy consumption is a function of dinitrogen selectivity, Faradaic efficiency, mass transfer limitations, reactor current density, and operating potential, and these factors along with the active metal(s) are the main cost drivers.

The goal of this work is to explore the potential for electrocatalytic reduction to competitively treat NO_3^--contaminated water in place of ion exchange (IX). We build on prior DFT results [28] by selecting five promising catalyst metals deposited on carbon cloth electrodes for evaluation of their NO_3^- reduction activity and Faradaic efficiency in a filterpress flow reactor presented in our prior work [30]. The metals are Ru, Ir, Co, and Cu, plus In based on its similarity to Cu regarding oxophilicity and use as a promoter metal in conventional catalytic NO_3^- reduction [31]. The filterpress reactor is used because in prior work [30] we demonstrated that reaction kinetics and not mass transfer limit overall reaction rates, and it can be plausibly scaled for water treatment [32]. The two best-performing catalysts (i.e., Cu and In) are then evaluated for the full range of reaction products, and for Cu, this motivates adding a second metal to overcome a stalled intermediate reaction. Longevity and regeneration of the best-performing electrodes are then explored, and the metal loadings and energy consumption are used to estimate costs for comparison to conventional catalytic treatment and IX. The results highlight that Cu amended with trace Pd achieves the highest Faradaic efficiency among the tested metals, a high activity, ammonia selectivity, and facile *in situ* regeneration, and that the cost for this technology is lower than conventional catalytic treatment and IX, the current go-to technology.

2. Experimental section

2.1. Reagents

All chemicals used are described in the Supporting Information (Text S1). All solutions were prepared in ultrapure water (18.2 MΩ·cm) produced by a Barnstead Nanopure system (Thermo Fisher Scientific).

2.2. Preparation of Ru/Ir/Co/In/In-Pd/Cu/Cu-Pd on activated carbon cloth (ACC) cathode

Kynol activated carbon cloth (ACC–5092–10) served as the working electrode support and was obtained from Gun EI Chemical Industry (Japan). A single metal (i.e., Ru, Ir, Co, In, or Cu) other than Pd was deposited using incipient wetness impregnation on a piece of ACC (hereafter referred to as M/ACC) that was cut to 2.5 cm × 2.0 cm (L × W; ∼0.1200 g). The desired concentration of each metal salt precursor solution was determined based on the pore volume of ACC and a target metal loading of ∼2 wt%, and the solutions were prepared by dissolving the corresponding metal salt in ultrapure water. An aliquot of the metal salt precursor solution that equals the pore volume was then added dropwise to ACC. A small amount of ethanol was used in some cases to prewet the ACC before adding the metal precursor solution to help distribute it evenly. The metal precursor loaded ACC was then placed in a tube furnace and dried in air at 60 °C for 12 h, calcined under N_2 flow, and reduced under H_2 flow both at 220 mL min^{-1} for 3 h and at an elevated temperature specific to the deposited metal. The calcination and reduction temperatures used for each metal are shown in Table S1. Bimetallic catalysts Cu–Pd and In–Pd were also deposited on the ACC, referred to as Cu–Pd/ACC and In–Pd/ACC, hereafter. For Cu and Pd deposition on Cu–Pd/ACC, the target Cu loading remained ∼2 wt% while the target Pd loadings were either 0.01 wt% or 0.1 wt%. Therefore, two $Pd(NO_3)_2$ solutions of different concentrations were required. After the ACC was loaded with the desired amount of $Cu(NO_3)_2$ solution and dried in air at 60 °C for 12 h, the corresponding Pd precursor solution was added to the ACC and dried in the same manner. The bimetal-loaded ACC was then calcined under N_2 flow and reduced under H_2 flow at 220 mL min^{-1} and 400 °C for 3 h, as with Cu/ACC. For In and Pd deposition on In–Pd/ACC, the target In loading was ∼2 wt% and the Pd loading was 0.01 wt%. The desired amount of $Pd(NO_3)_2$ solution was first loaded on the ACC, dried in air at 60 °C for 12 h, calcined under N_2 flow and reduced under H_2 flow both at 220 mL min^{-1} and 400 °C for 3 h. The Pd deposited ACC was then loaded with $In(NO_3)_3$ solution, air dried and calcined the same way as for Pd, and reduced under H_2 flow at 220 mL min^{-1} and 120 °C for 3 h. As a control, a 1 wt% Pd 0.1 wt% In/ACC electrode (referred to as Pd–In/ACC) evaluated in prior work [30] was also synthesized following the same method.

2.3. Electrocatalytic nitrate reduction experiments

2.3.1. Nitrate reduction experiments in filterpress flow reactor

The electrocatalytic nitrate reduction experiments were conducted in the filterpress flow reactor evaluated for electrocatalytic nitrite reduction in our prior work [30]. The M/ACC served as the cathode, and IrO_2 on carbon paper (Dioxide Materials, FL) served as the anode. The reference electrode (RE) was a Ag/AgCl electrode in 1.0 M KCl solution, which has a thermodynamic potential of 0.222 V vs. standard hydrogen electrode (SHE). The cathode was placed above the cathodic chamber and the anode below the anodic chamber, respectively. Each chamber consisted of a 1-mm Teflon sheet with a cavity as the flow channel and the cathodic and anodic chambers were separated by a Nafion 117 cation-exchange membrane. The reactor was operated in recirculation mode unless otherwise stated. A 40-mL solution initially containing 100 mg L^{-1} NO_3^- and 1.0 M phosphate buffer (pH 6.5 ± 0.1, 0.55:0.45 molar ratio of KH_2PO_4 and K_2HPO_4, degassed under vacuum for 15 min before use) was pumped into the cathodic chamber of the reactor while another 40-mL solution with only 1.0 M phosphate buffer was pumped into the anodic chamber. The effluent from both chambers was circulated back to their respective reservoirs and well mixed with their remaining solutions using magnetic stir bars. Based on prior results [30], the 1.0 M phosphate buffer was selected over other buffer systems (i.e., 0.1 M phosphate buffer with and without constant CO_2 bubbling) because it ensured a relatively constant solution pH during reactions (in contrast to the 0.1 M phosphate buffer) and did not significantly inhibit the catalytic activity (in contrast to CO_2 bubbling). We also observed minimal differences in normalized activity, Faradaic efficiency, and energy consumption at different buffer concentrations (1.0 M versus 0.02 M phosphate buffer) with the synthesized electrode in this study (Table S2). Note that the 1.0 M buffer concentration might not be directly relevant to drinking water treatment conditions, but provides controlled water chemistry conditions that promotes mechanistic understanding of the factors controlling electrocatalytic performance. Further studies evaluating more relevant drinking water treatment conditions are warranted for technology development for practical adoption. A Gamry 1010E potentiostat (Warminster, PA) was connected to the reactor and a desired potential was applied between the as-synthesized M/ACC cathode and the reference electrode. A common reduction experiment lasted for 2 h while the current on the cathode was recorded. Samples were taken regularly from the cathodic reservoir for the analysis of NO_3^-, NO_2^-, NH_2OH, and NH_4^+ concentrations. The metal residual concentrations in the cathodic solution at the end of selected 2-h experiments were analyzed by ICP-MS. Meanwhile, full cell potentials between the cathode and the anode at all sampling times were recorded and averaged throughout the 2-h experiment to calculate the energy consumption. In general, potentials used in reduction experiments were equal to or slightly greater than the hydrogen evolution reaction (HER) potentials on the corresponding cathodes determined from multistep chronoamperometry results to maximize Faradaic efficiency. An extended range of potentials was applied on the Cu/ACC cathode in order to validate the effect of potential on Faradaic efficiency. Longevity of the best-performing cathodes was investigated by conducting multiple cycles of 2-h experiments in series. Regeneration of the cathode was performed by either applying a constant potential beyond the HER onset potential of the metal of interest on the corresponding cathode in 1.0 M phosphate buffer solution without nitrate addition, or heating the used cathodes under H_2 flow at its synthesis temperature. All potentials applied were converted to and presented against reversible hydrogen electrode (RHE). The conversion was carried out according to Eq. 1:

$$E_{(\mathrm{RHE})} = E_{(\mathrm{Ag/AgCl})} + 0.222\ \mathrm{V} + 0.059 \times \mathrm{pH} \tag{1}$$

2.3.2. Nitrate reduction experiments in H-Cell for gaseous product analysis

For several best-performing cathodes, electrocatalytic nitrate reduction was carried out in a gas tight H-cell (Dek Research) with ^{15}N labelled $^{15}NO_3^-$ as the reactant to detect the formation of gaseous products. The cathode, anode, reference electrode, cation exchange membrane, and the concentrations of buffer solution and $^{15}NO_3^-$ were the same as in the flow reactor. Solution mixing was provided in both cathodic and anodic chambers using stir bars at 500 rpm. Solution volume in both chambers was reduced to 35 mL to provide enough headspace for gas sampling. Before each reaction started, 1 mL headspace in the cathodic chamber was replaced with the same amount of Ar as an indicator for leakage. During sampling, 100-μL gas samples were taken from the headspace and analyzed for ^{15}NO, $^{15}N_2O$, $^{15}N_2$, and Ar. A 0.3-mL aqueous sample was simultaneously taken for nitrate, nitrite, hydroxylamine, and ammonium analysis.

2.3.3. Analytical methods

Nitrate and nitrite concentrations were analyzed using ion chromatography (IC, Dionex ICS-2100) equipped with a Dionex IonPac AS19 column. The eluent was KOH solution (12.5–45 mM), and the flow rate was 1 mL min^{-1}. Ammonium concentrations were determined using Hach colorimetric kits (salicylate method, low range, 0.02–2.5 mg L^{-1} NH_4^+–N). Hydroxylamine (NH_2OH) was first derivatized according to Kumar et al. [33] to allow for UV detection after high-performance liquid chromatography (HPLC). Detailed derivatization and detection methods are described in Text S1. Gaseous products (i.e., ^{15}NO, $^{15}N_2O$, $^{15}N_2$, and Ar) in H-cell experiments were analyzed by an Agilent Technologies 5977 A gas chromatography/mass spectrometer (GC/MSD) equipped with a Varian Plot CP-Molsieve 5 Å column (25 m × 0.25 mm). The oven temperature was 165 °C and helium was the carrier gas at a flow rate of 1.0 mL min^{-1}.

2.3.4. Key parameter calculations

Key parameters for electrode performance evaluation include NO_3^- reduction activity, NO_2^-, NH_2OH, NH_4^+ and N_2 selectivity, Faradaic efficiency, and energy consumption.

Activity was represented by a normalized apparent pseudo-first-order rate constant. The rate constants were obtained from a linear regression of the natural log of NO_3^- concentration in the cathodic reservoir versus time plots for up to 50 % NO_3^- conversion and were then normalized to the total mass of the catalyst metals on the M/ACC and the volume of the cathodic solution.

NO_2^- selectivity ($S_{NO_2^-}$) was calculated by Eq. 2:

$$S_{NO_2^-}\ (\%) = \frac{C_{NO_2^-,\ \mathrm{final}}}{C_{NO_3^-,\ \mathrm{initial}} - C_{NO_3^-,\ \mathrm{final}}} \times 100 \tag{2}$$

NH_2OH selectivity (S_{NH_2OH}) was calculated by Eq. 3:

$$S_{NH_2OH}\ (\%) = \frac{C_{NH_2OH,\ \mathrm{final}}}{C_{NO_3^-,\ \mathrm{initial}} - C_{NO_3^-,\ \mathrm{final}}} \times 100 \tag{3}$$

NH_4^+ selectivity ($S_{NH_4^+}$) was calculated by Eq. 4:

$$S_{NH_4^+}\ (\%) = \frac{C_{NH_4^+,\ \mathrm{final}}}{C_{NO_3^-,\ \mathrm{initial}} - C_{NO_3^-,\ \mathrm{final}}} \times 100 \tag{4}$$

where $C_{NO_2^-,\ \mathrm{final}}$, $C_{NH_2OH,\ \mathrm{final}}$ and $C_{NH_4^+,\ \mathrm{final}}$ are the final NO_2^-, NH_2OH, and NH_4^+ concentrations (mM) in the cathodic solution, and $C_{NO_3^-,\ \mathrm{initial}}$ and $C_{NO_3^-,\ \mathrm{final}}$ are the initial and final concentrations (mM) of NO_3^-, respectively. In all H-cell experiments using $^{15}NO_3^-$ as the reactant, ^{15}NO and $^{15}N_2O$ were never detected by GC/MS. Thereafter, they were excluded from product analysis and selectivity calculation.

$^{15}N_2$ was the remaining product detected by GC/MS in the H-cell experiments. N_2 selectivity (S_{N_2}) was calculated by Eq. 5:

$$S_{N_2}\ (\%) = \frac{C_{N_2,\ \mathrm{final}}}{C_{NO_3^-,\ \mathrm{initial}} - C_{NO_3^-,\ \mathrm{final}}} \times 100 \tag{5}$$

where $C_{N_2,\ \mathrm{final}}$ is the final N_2 concentration (mM as N) assuming all $^{15}N_2$ formed from $^{15}NO_3^-$ reduction (present in both headspace and solution) was dissolved in the cathodic solution. The Henry's constant was used to calculate $C_{N_2,\ \mathrm{final}}$ from the N_2 concentration in the headspace measured by GC/MS.

Since the $^{15}NO_3^-$ reduction in the H-cell established a complete N mass balance, N_2 concentrations were not measured for experiments conducted in the filterpress flow reactor, and the difference between the amount of reduced NO_3^- and formed NO_2^-, NH_2OH, and NH_4^+ was attributed to N_2 formation. Therefore, the apparent dinitrogen gas selectivity (S_{N_2}) in the flow reactor was calculated by Eq. 6:

$$S_{N_2}\ (\%) = 100 - S_{NO_2^-} - S_{NH_2OH} - S_{NH_4^+} \tag{6}$$

Faradaic efficiency (FE) was calculated by Eq. 7:

$$\mathrm{FE}(\%) = \frac{F \times \sum_i S_i \times z_i \times (C_{NO_3^-,\mathrm{initial}} - C_{NO_3^-,\mathrm{final}}) \times V}{\sum_{t=0}^{t=7200} I_t \times \Delta t} \times 100 \tag{7}$$

where F is the Faraday constant (i.e., 96,485 C mol^{-1}), S_i is the selectivity defined above, z_i is the moles of electrons transferred per mole of NO_3^- reduced to the product i, V is the total volume of the cathodic solution in the reservoir (i.e., 0.04 L), I_t is the current (A) measured at time t (s), and Δt is the time interval between each current measurement. The summation in the denominator represents the total charge (C) passing the working electrode during the 2-h reduction experiment.

Energy consumption (EC) was calculated by Eq. 8:

$$\mathrm{EC}\ \left(\mathrm{kWh\ mol^{-1}\quad NO_3^-}\right) = \frac{E \times \dfrac{\sum_{t=0}^{t=7200} I_t \times \Delta t}{3600000}}{\left(C_{\mathrm{NO_3^-},\ \mathrm{initial}} - C_{\mathrm{NO_3^-},\ \mathrm{final}}\right) \times V} \tag{8}$$

where E is the average full cell potential (V) between the cathode and the anode measured with a portable voltmeter throughout the 2-h reduction experiment.

2.4. Electrode characterization

Bulk metal loadings on all cathodes synthesized were measured using acid digestion followed by inductively-coupled plasma–optical emission spectroscopy or mass spectrometry (ICP-OES or ICP-MS). Crystallinity of catalyst metals deposited on all cathodes were analyzed using powder X-ray diffraction (PXRD). Multistep chronoamperometry (CA) was used to obtain the current-potential relationship of each synthesized cathode. Low-resolution transmission electron microscopy (LR-TEM) images, high-resolution TEM (HR-TEM) images, high angle annular dark field (HAADF) images, energy-dispersive X-ray spectroscopy (EDS) spectra,

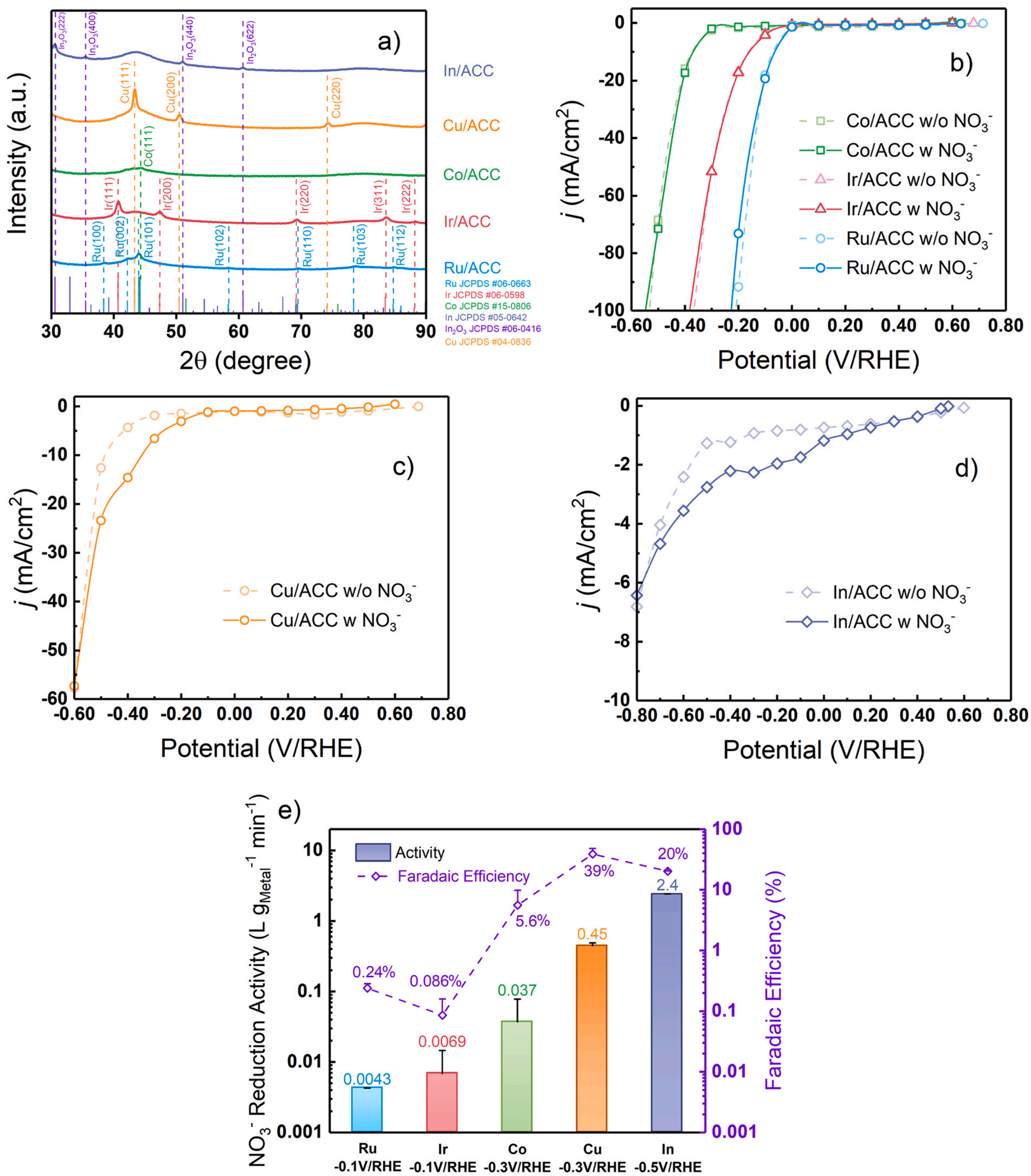

Fig. 1. a) PXRD patterns of Ru/ACC, Ir/ACC, Co/ACC, Cu/ACC, and In/ACC. Current-potential curves of b) Ru/ACC, Ir/ACC, Co/ACC, c) Cu/ACC, and d) In/ACC in 1.0 M phosphate buffer and with 15 mM NO_3^- addition at 40 mL min^{-1} in the filterpress flow reactor. e) Apparent pseudo-first-order rate constants and Faradaic efficiencies of the five monometallic electrodes at 40 mL min^{-1} in the filterpress flow reactor.

and X-ray photoelectron spectroscopy (XPS) spectra were obtained for Cu/ACC, Cu-Pd/ACC, In/ACC, and In-Pd/ACC electrodes. Details about sample preparation, experimental conditions and procedures, and data analysis for all characterization techniques performed are presented in Text S1.

3. Results and disscussion

3.1. Voltametric evaluation of monometallic electrodes (M/ACC)

The five catalyst metals of interest (i.e., Ru, Ir, Co, Cu, and In) were successfully deposited on the activated carbon cloth (ACC) using incipient wetness impregnation as indicated by the PXRD patterns as shown in Fig. 1a. The characteristic peaks in the PXRD patterns for Ru/ACC, Ir/ACC, Co/ACC, and Cu/ACC match those in the reference patterns of their respective metals. For these metals, no diffraction peaks for metal oxides or other species are observed. However, the characteristic diffraction peaks of In/ACC at 30.56°, 35.45°, 37.62°, 50.99°, and 60.69° do not match the diffraction peaks in the In metal reference (JCPDS #05–0642) but those in the In_2O_3 reference (JCPDS #06–0416). This indicates that indium was mainly present on the electrode as In_2O_3 likely due to the low reduction temperature of 120 °C (Table S1), which was intentionally used for indium deposition to prevent loss via formation of volatile indium species [34]. Inhibition in nitrate reduction activity of the In/ACC electrode was not expected as many studies reported the presence of In_2O_3 in In/In_2O_3 catalysts reduced similarly at 120 °C for (electro)catalytic nitrate reduction [26,35–37].

Current-potential curves of the synthesized monometallic electrodes were acquired using multistep chronoamperometry and are shown in Fig. 1b. The current-potential curves for Ru/ACC and Ir/ACC start to drop between –0.10 V/RHE and 0 V/RHE when no NO_3^- is present in the solution (light dashed lines), indicating the onset of HER. The HER onset is around –0.30 V/RHE for both Co/ACC (Fig. 1b) and Cu/ACC (Fig. 1c), and –0.50 V/RHE for In/ACC (Fig. 1d). When NO_3^- is added in the solution, the current (dark solid lines) for Ru/ACC, Ir/ACC and Co/ACC does not show a noticeable increase when compared to the current measured in absence of NO_3^- (light dashed lines, Fig. 1b), indicating no significant NO_3^- reduction occurred on these electrodes. On the other hand, the current after NO_3^- addition increased for Cu/ACC and In/ACC compared to when no NO_3^- was present. This increase is attributed to NO_3^- reduction and it occurred at around –0.20 V/RHE and –0.10 V/RHE on Cu/ACC and In/ACC, respectively, before the onset of HER. As the potential moved negatively from the onset of NO_3^- reduction to the onset of HER, the NO_3^- reduction currents increase, suggesting increasing activity for both electrodes while HER currents remain relatively constant. These trends in current indicate a high current ratio (CR), which is calculated from the difference in current with and without NO_3^- present divided by the current with NO_3^- present via Eq. 9:

$$CR = \frac{I_{wNO_3^-} - I_{w/oNO_3^-}}{I_{wNO_3^-}} \quad (9)$$

where $I_{w\,NO_3^-}$ is the current (A) measured with NO_3^- addition (representing total current mainly resulting from NO_3^- reduction and HER) and $I_{w/o\,NO_3^-}$ is the current (A) measured without NO_3^- addition (representing only HER current) of the electrodes. The difference between $I_{w\,NO_3^-}$ and $I_{w/o\,NO_3^-}$ is attributed to the NO_3^- reduction current alone. The closer CR is to 1, the higher the Faradaic efficiency. CRs for Cu/ACC and In/ACC at multiple potentials are listed in Table S3. As the potential moved negatively from the onset of NO_3^- reduction to the onset of HER, the CR (and thus, Faradaic efficiency) of Cu/ACC reached a peak at –0.30 V/RHE and dropped once past the HER onset potential. The CR of In/ACC reached a peak at –0.30 V/RHE, remained constant until the HER onset potential of –0.50 V/RHE, and dropped afterwards. Based on the NO_3^- reduction current and CR trends, we speculated that for any potentially active electrode, its optimal operating potential with simultaneous fast kinetics and high Faradaic efficiency should be near its HER onset potential. In addition, keeping the operating potential below the HER onset potential also avoids operational difficulty caused by gas bubbling and associated current fluctuations that occur when bubbles contact the cathode surface.

3.2. Activity and Faradaic efficiency of monometallic electrodes

Electrocatalytic NO_3^- reduction was next evaluated at constant potentials in the custom-made filterpress flow reactor. We first measured Cu/ACC reduction at several different applied potentials to test our assumption that the operating potential that maximizes activity with Faradaic efficiency is near the HER potential when CR is at a maximum, and results are presented in Figure S1a. The highest rate constant was 0.85 L g_{Cu}^{-1} min^{-1}, observed at –0.40 V/RHE, which is twice the rate constant at –0.30 V/RHE (i.e., 0.45 L g_{Cu}^{-1} min^{-1}) and more than 10 times the values when the potential was even more positive. The maximum FE coincides with the maximum CR at –0.30 V/RHE. In/ACC also showed a much lower activity at –0.30 V/RHE (i.e., 0.016 L g_{In}^{-1} min^{-1}, Figure S1c) than –0.50 V/RHE (i.e., 2.4 L g_{In}^{-1} min^{-1}) and Cu/ACC at –0.30 V/RHE (i.e., 0.45 L g_{Cu}^{-1} min^{-1}). Hence, setting the potential at the maximum CR appears to maximize activity and/or FE and allows comparison of electrodes under their best conditions. This motivated us to next evaluate nitrate reduction for the five metals at potential values that maximized CR and are near HER onset potentials. This corresponds to –0.10, –0.10, –0.30, –0.30, and –0.50 V/RHE for Ru/ACC, Ir/ACC, Co/ACC, Cu/ACC, and In/ACC, respectively, and results are presented in Fig. 1e. As expected, Cu/ACC and In/ACC have the top reaction rate constants (0.45 L g_{Cu}^{-1} min^{-1} and 2.4 L g_{In}^{-1} min^{-1}, respectively) and Faradaic efficiencies (i.e., 39 % and 20 %, respectively) among all five monometallic electrodes evaluated. Cu/ACC has a higher FE but a lower activity, while In/ACC has a higher activity but lower FE. Contrary to the DFT prediction (that motivated our initial metal selection) [28], but consistent with the above voltametric analysis, Ru/ACC, Ir/ACC, and Co/ACC had NO_3^- reduction activities more than an order of magnitude lower than Cu/ACC and In/ACC near their respective HER onset potentials. Also, their FE were low, with Co at 5.6 %, and Ru/ACC and Ir/ACC below 0.5 %. Note that Co- and Ru-based catalysts have been found to be active and efficient for electrocatalytic nitrate reduction [38–41]. The lower-than-expected activity of Co/ACC and Ru/ACC observed is experimentally specific to this work, given the consideration to avoid strong HER during reactor operation and balance the NO_3^- reduction activity and FE as mentioned above. Besides, a Pd–In/ACC was also synthesized and tested as a control because Pd has been widely studied for electrocatalytic NO_3^- reduction, and this combination has shown promises for both catalytic NO_3^- reduction and electrocatalytic NO_2^- reduction in previous studies [30,42]. However, Figure S1b shows that Pd–In/ACC only became active at or below –0.60 V/RHE with less than 3 % Faradaic efficiency due to strong HER, indicating Pd–In/ACC is not a simultaneously active and efficient electrocatalyst for NO_3^- reduction, and hereafter, will only be considered for cost comparison with catalytic treatment in the following section.

Importantly, NO_3^- reduction activities for Cu/ACC and In/ACC are comparable to or higher than literature values [43] for electrocatalytic NO_3^- reduction and for catalytic NO_3^- reduction in well-mixed batch systems (Table S4), and there are no prior reports of high activity for electrocatalytic NO_3^- reduction using a monometallic In-based catalyst alone. Although not commonly presented in the literature, cost-normalized activities for all the electrodes tested in this study are also presented in Table S5 for future comparison with other studies. Cu/ACC and In/ACC still have the top cost-normalized activities due to their high intrinsic activities and low metal costs. Faradaic efficiencies are rarely reported for Cu-based electrocatalytic reduction of NO_3^- in flow reactors, and our value is comparable to the few reported values available [44–48]. There are no prior reports of FE for In-based systems in a flow reactor.

3.3. Cu/ACC and In/ACC electrode characterization

Cu/ACC and In/ACC electrodes were further characterized to probe properties associated with their high activity and FE. TEM images of Cu/ACC (Figure S2a) and In/ACC (Figure S2b) showed Cu and In_2O_3 particles were on average 7.4 ± 5.1 nm and 14.6 ± 3.1 nm in size, respectively. Particle sizes were greater for In_2O_3 as O atoms were incorporated into crystal lattices. Cu nanoparticles have a wider size distribution and more irregular shape, while In_2O_3 nanoparticles are more uniform in size and have a more regular cubic shape, similar to other studies [49]. Per ICP analysis (Table S6), average Cu and In loadings are slightly lower than the target 2 wt%, 1.4 ± 0.26 wt% for Cu (N = 5) and 1.5 ± 0.65 wt% for In (N = 6). However, the low standard deviation indicates the metal deposition is reproducible. X-ray photoelectron spectroscopy (XPS) and Auger electron spectroscopy (AES) were used to characterize the surface element oxidation states of Cu/ACC and In/ACC. Two major peaks were observed at 932.7 eV and 952.8 eV in Cu 2*p* XPS spectrum for Cu/ACC (Figure S2c), representing Cu $2p_{3/2}$ and Cu $2p_{1/2}$ peaks, respectively. Deconvolution of the Cu $2p_{3/2}$ peak revealed one Cu^0/Cu^+ sub-peak at 932.7 eV, one Cu^{2+} sub-peak, likely due to $Cu(OH)_2$, at 934.9 eV, and two satellite peaks above 941 eV indicating the presence of Cu^{2+}. All of these peaks match the Cu 2*p* peaks reported for Cu-based references [50]. Although the Cu^0 and Cu^+ peaks were too close to tell in Cu 2*p* spectrum for Cu/ACC, the differentiation of the two species was made from the Cu LMM Auger spectrum (Figure S2e). It shows a maximum peak intensity at 918.1 eV corresponding to Cu^0 [50] whereas no Cu^+ peak was observed at 917.0 eV. The presence of the Cu^{2+} peak and the satellite peaks indicate Cu surfaces might be oxidized to some degree, as also evidenced by the O 1 *s* peak at 531.3 eV corresponding to $Cu(OH)_2$ observed in the O 1 *s* XPS spectrum (Figure S2d) [51] and Cu LMM Auger peak at 916.4 eV (Figure S2e) [50]. However, given that the maximum peaks in both Cu 2*p* XPS spectrum and Cu LMM Auger spectrum for Cu/ACC were attributed to Cu^0, and that no other peaks for Cu_2O or CuO were observed in the Cu 2*p* and O 1 *s* spectra (and the PXRD pattern) for Cu/ACC, we believe Cu^0 was the dominant species while only limited surface oxidation to $Cu(OH)_2$ occurred. This suggests Cu^0 was likely responsible for the activity of electrocatalytic NO_3^- reduction on Cu/ACC.

The In 3*d* XPS spectrum for In/ACC is shown in Figure S2f. The In $3d_{5/2}$ and In $3d_{3/2}$ peaks were observed at 445.2 eV and 452.7 eV, respectively. Deconvolution of the In $3d_{5/2}$ peak resulted in three sub-peaks at 443.3 eV, 445.0 eV and 445.6 eV that were assigned to In^0, In_2O_3 and $In(OH)_3$, respectively. The In^0 peak is only 1.0 % of the In $3d_{5/2}$ peak, possibly due to the low reduction temperature that was unable to fully reduce In_2O_3 to In^0. The minimal amount of In^0 also suggests NO_3^- reduction activity mainly comes from In^{3+} species, either In_2O_3 or $In(OH)_3$.

3.4. End-product selectivity

3.4.1. End-product selectivity of Cu/ACC and In/ACC

The formation of various NO_3^- reduction intermediates and products including NO_2^-, NO, N_2O, N_2, NH_2OH, and NH_4^+ with Cu- and In-based electrodes was probed in batch reduction experiments using a gastight H-cell with ^{15}N labelled NO_3^- as the reactant. Results in Figure S3 show that a nitrogen mass balance was established with Cu/ACC at all sampling times, and for In/ACC only at the end of the reaction time. The major reaction products were NO_2^-, NH_2OH, and NH_4^+, with only minor amounts of N_2, and no detection of NO and N_2O. The lack of a nitrogen mass balance for In/ACC at earlier times suggests there are sorbed intermediates that are eventually converted to the measured products. Therefore, in the flow reactor experiments, we only measured NO_2^-, NH_2OH, NH_4^+, and attribute the remaining products to N_2 only after NO_3^- conversion is complete.

End-product selectivity for Cu/ACC and In/ACC in the filterpress flow reactor at the optimal potentials are presented in Fig. 2a, along with end-product selectivity of Cu/ACC at other potentials. The NH_4^+ selectivity for Cu/ACC at –0.30 V/RHE is as high as 91 %. It decreases with increasing potential (down to 11 % at 0.00 V/RHE), with NO_2^- as a rate-limiting intermediate, but shows little change with decreasing potential. These trends are logical, as more negative potentials correspond to faster reduction and more atomic hydrogen (H·) surface coverage, the latter favoring NO hydrogenation over N–N coupling [42]. In contrast to Cu/ACC, In/ACC showed mixed selectivity for NH_4^+ (40 %), NH_2OH (37 %) and N_2 (22 %), with very little NO_2^- (1.4 %). NH_2OH is an intermediate that will convert to NH_4^+ with prolonged reaction time. Therefore, although In/ACC shows higher activity than Cu/ACC for NO_3^- reduction, its application could be limited by slow transformation of NH_2OH.

3.4.2. Bimetallic catalyst deposition to address electrode selectivity concerns

To address NO_2^- and NH_2OH accumulation during NO_3^- reduction with Cu/ACC and In/ACC, respectively, Pd was added to these electrodes. The rationale was that although Pd alone has low activity for electrocatalytic NO_3^- reduction based on the similar currents achieved with and without the presence of nitrate in the solution within the potential range tested (Figure S1d), it is highly active for electrocatalytic NO_2^- reduction, and no build-up of NH_2OH has been observed with Pd–In catalysts, per our previous work [30]. However, Pd is also very active for HER as indicated by the large current shown in Figure S1d, and with more Pd more HER is anticipated. Therefore, only trace amounts of Pd (relative to the amount of Cu or In present) were added. The incipient wetness impregnation method was used to deposit Pd at 0.01 wt% and 0.1 wt% to Cu–Pd/ACC, and at 0.01 wt% to In–Pd/ACC. ICP analysis confirmed the average Cu, In and Pd loadings are close to the nominal values on the respective electrodes (Table S6). The two Cu–Pd/ACC electrodes are referred to as Cu 0.01 % Pd/ACC and Cu 0.1 % Pd/ACC, and the In–Pd/ACC electrode is referred to as In 0.01 % Pd/ACC. PXRD (Figure S4), XPS (Figure S5 and S6), and LR-TEM (Figure S7a, S8a and S9a) results of Cu–Pd/ACC and In–Pd/ACC show similar diffraction patterns, surface oxidation states, particle size distributions and shapes compared to the Cu/ACC and In/ACC, respectively. Pd deposition on all bimetallic electrodes was confirmed by XPS (for Cu–Pd/ACC) and STEM-EDS (for Cu–Pd/ACC and In–Pd/ACC). A detailed description of electrode characterization is provided in Text S2.

Electrocatalytic NO_3^- reduction was performed on the Cu–Pd/ACC electrodes at –0.30 V/RHE and –0.20 V/RHE, and on the In–Pd/ACC electrode at –0.50 V/RHE. The end-product selectivity of the Cu–Pd/ACC electrodes is shown in Fig. 2b. At both potentials, Pd addition to Cu/ACC greatly reduced NO_2^- accumulation, and increased NH_4^+ selectivity. Notably, Cu 0.01 % Pd/ACC achieved an excellent NH_4^+ selectivity of 98.7 % at –0.30 V/RHE. Also, as shown in Fig. 2c, NO_3^- reduction activity at both potentials almost doubles and triples with 0.01 wt% and 0.1 wt% Pd addition to Cu/ACC, respectively. The decreasing Tafel slopes (Table S7) calculated for Cu/ACC and Cu–Pd/ACC with increasing Pd addition coincide with the activity trend and support that Pd addition promotes electrocatalytic nitrate reduction. The high Tafel slope (i.e., 313 mv/decade) for Cu/ACC also indicates that electrocatalytic nitrate reduction on Cu follows a chemical-electrochemical mechanism with the rate determining step (RDS) to be the chemical process (i.e., NO_3^- adsorption [11]). The RDS transitions from the chemical process to a single-electron electrochemical process for Cu–Pd/ACC, as indicated by the decreasing Tafel slopes approaching the theoretical value for a single-electron electrochemical reaction (i.e., 120 mV/decade) with increasing Pd addition. Also, the FE increases to 45 % with 0.01 wt% Pd addition to Cu/ACC but decreases to 18 % with 0.1 wt% Pd addition. The FE result indicates that HER became too active at the higher Pd loading. Hence, 0.01 % Pd addition to Cu/ACC

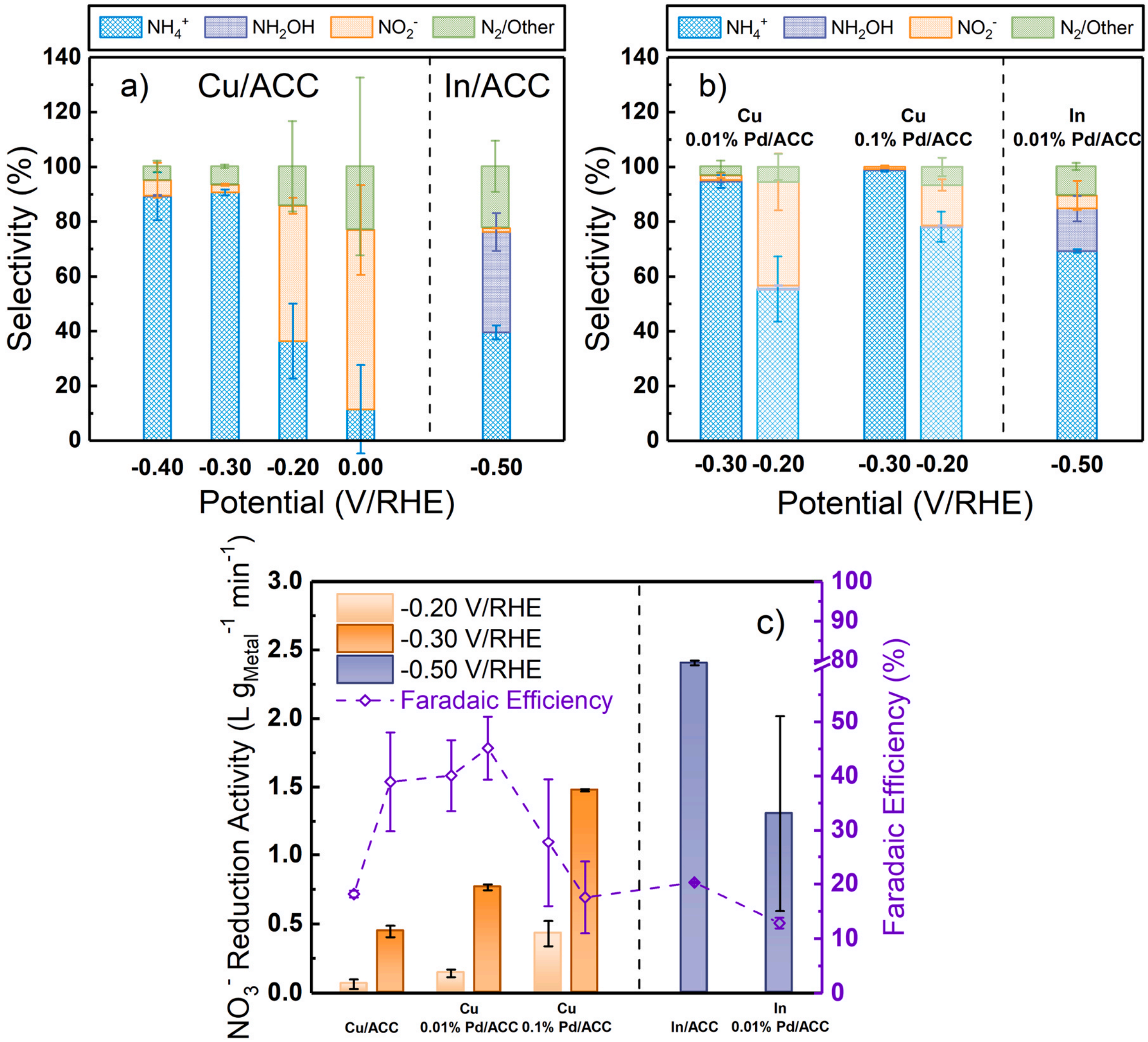

Fig. 2. End-product selectivity of electrocatalytic NO_3^- reduction for a) Cu/ACC from –0.40 V/RHE to 0.00 V/RHE, and In/ACC at –0.50 V/RHE, and b) Cu 0.01 % Pd/ACC and Cu 0.1 % Pd/ACC at –0.30 and –0.20 V/RHE, and In 0.01 % Pd/ACC at –0.50 V/RHE in the filterpress flow reactor with a flow rate of 40 mL min^{-1}. c) Apparent pseudo-first-order rate constants and Faradaic efficiencies of electrocatalytic NO_3^- reduction for Cu/ACC, Cu 0.01 % Pd/ACC, and Cu 0.1 % Pd/ACC at –0.30 and –0.20 V/RHE, and In/ACC and In 0.01 % Pd/ACC at –0.50 V/RHE in the filterpress flow reactor with a flow rate of 40 mL min^{-1}.

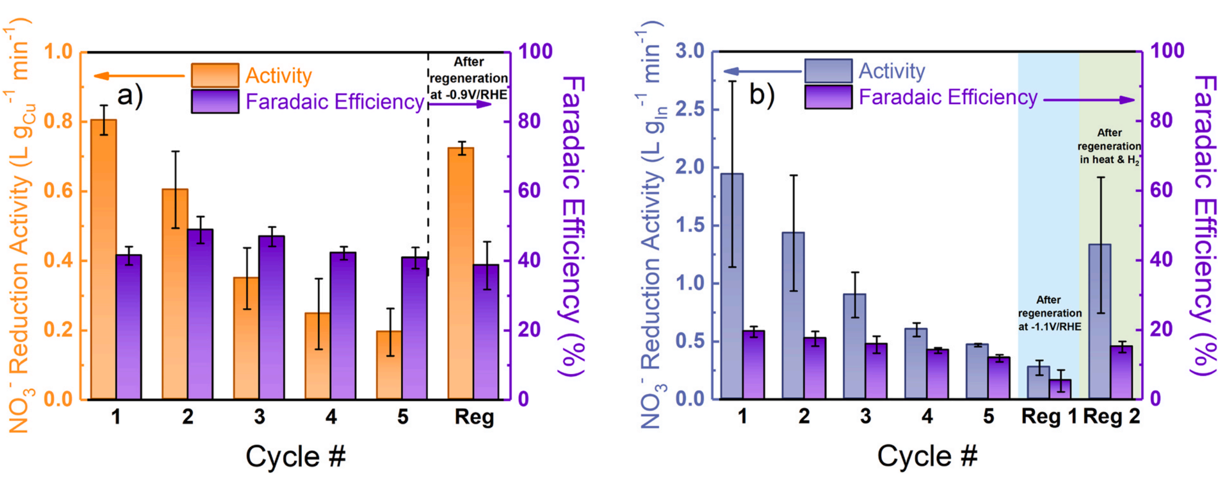

Fig. 3. Apparent pseudo-first-order rate constants and Faradaic efficiencies for multiple cycles of electrocatalytic NO_3^- reduction a) using Cu 0.01 % Pd/ACC at an applied potential of −0.30 V/RHE and regenerated after the 5th cycle by applying a potential of −0.90 V/RHE; b) using In/ACC at an applied potential of −0.50 V/RHE and regenerated after the 5th cycle by applying a potential of −1.1 V/RHE and by heating the electrode under H_2 flow at 120 °C for 1 h. The flow rate is 40 mL min^{-1} in the filterpress flow reactor.

addresses NO_2^- accumulation, while simultaneously increasing activity and FE.

Pd addition to In/ACC also reduced NH_2OH accumulation, from 37 % to 15 %, while simultaneously reducing N_2 selectivity from 22 % to 10 %, and increasing NH_4^+ selectivity from 40 % to 69 %, as shown in Fig. 2b. However, benefits to activity and FE did not occur as with Cu/ ACC. Instead, with Pd addition to In/ACC the activity decreased by 50 %, and the FE decreased from 20 % to 13 %. The FE results suggests that the excess H_2 generated by adding Pd could not be offset by the extra H_2 consumed for NH_2OH reduction to NH_4^+. Therefore, Pd addition to In/ACC does not provide an overall benefit.

3.5. Longevity and regeneration of Cu 0.01 % Pd/ACC and In/ACC electrodes

The best-performing Cu 0.01 % Pd/ACC and In/ACC electrodes were subject to repeated reaction cycles to evaluate longevity and stability at their optimal reduction potentials. As shown in Fig. 3, both Cu 0.01 % Pd/ACC and In/ACC exhibit similar patterns of activity loss. The Cu 0.01 % Pd/ACC maintained 25 % of its original activity after 5 cycles compared to 24 % for In/ACC. The Faradaic efficiencies did not decrease as much; Cu 0.01 % Pd/ACC maintained 86 % of the original Faradaic efficiency after 5 cycles while In/ACC maintained 61 %. Cu, Pd and In leaching were measured during reduction, with results presented in Figure S10. Less than 0.1 % of total Cu leached and the average concentration in the cathodic solution was 22 μg L^{-1} after each cycle, much lower than the 1.3 mg L^{-1} MCL of Cu in drinking water [6]. No Pd leaching was detected. Approximately 1.5 % of the In on the tested piece of In/ACC leached and the average concentration in the cathodic solution was 814 μg L^{-1} after each cycle. This is much higher than Cu, although the U.S. EPA does not regulate the amount of In in drinking water. Also, the greater In leaching contradicts a previous finding that In leaches less than Cu when used as a promoter metal for catalytic NO_3^- reduction [35].

After 5 cycles, both electrodes were regenerated by applying a constant potential to the electrode in electrolyte without NO_3^-. In replicate experiments after 5 cycles, the In/ACC electrode was also regenerated by heating under H_2 flow at the temperature used during electrode synthesis (i.e., 120 °C). Electrochemical regeneration is preferred because it is performed *in situ* and does not require disassembling and reassembling the reactor. For Cu 0.01 % Pd/ACC (Fig. 3a), 90 % of the activity in the 1st cycle was recovered after applying a potential of −0.90 V/RHE for 2 h, and the FE remained unchanged. Also, NH_4^+ selectivity recovered from 66 % to 77 % (Figure S11a) after the regeneration. By contrast, no activity was recovered for In/ACC after applying a potential of −1.1 V/ RHE for 1 h, and the FE (Fig. 3b), NH_4^+ selectivity (Figure S11b) further decreased. Alternatively, for this same electrode, 68 % of the activity in the 1st cycle was recovered after heating the electrode under H_2 flow at 120 °C for 1 h (Fig. 3b). However, the end-product distribution after heat regeneration (Figure S11b) is more similar to that of the 2nd cycle, suggesting H_2 heat treatment might only partially regenerate the In/ ACC.

As Cu 0.01 % Pd/ACC showed promise for *in situ* regeneration, a prolonged reduction experiment involving 12 reduction cycles at −0.30 V/RHE and 3 regeneration cycles at −0.90 V/RHE was performed to further characterize electrode longevity. The three regeneration cycles were conducted after the 5th, 8th, and 11th reduction cycles, respectively. Figure S12a shows NO_3^- reduction activity decreased over repeated reduction cycles. The activity recovered to 117 % and 87 % of the original activity after the first two regeneration cycles, respectively, compared with 61 % after the third regeneration. The lowest activity observed among the 12 reduction cycles was 52 % of the original activity. Faradaic efficiency was over 44 % before the 1st electrode regeneration and maintained around 30 % afterwards. NH_4^+ selectivity decreased over repeated reduction cycles (Figure S12b). NH_4^+ remained the main product at 70 % in Cycle 12 which had the lowest NH_4^+ selectivity, and electrode regeneration was shown to help regain NH_4^+ selectivity after the first two regeneration cycles.

XPS and/or Auger electron spectroscopy were performed on the Cu 0.01 % Pd/ACC and In/ACC electrodes before reaction, after 5 reaction cycles, and after regeneration to interpret mechanisms of electrode deactivation and regeneration. For Cu 0.01 % Pd/ACC, all three Cu 2*p* XPS spectra before reaction, after 5 cycles, and after regeneration (Figure S5a) were similar, with two major peaks for Cu^0/Cu^+ and Cu^{2+}. However, a shift in dominant species of Cu 0.01 % Pd/ACC from Cu^0 before reaction to Cu^{2+} after 5 reaction cycles and after regeneration was observed as indicated by the kinetic energy of the maximum peak intensity in Cu LMM Auger spectra (Figure S5d). Given that a lattice oxygen peak evolved after 5 cycles in the O 1 *s* spectra of Cu 0.01 % Pd/ ACC, we believe the activity loss results from the formation of Cu^{2+} oxides. The relative intensity of the lattice oxygen peak decreased after regeneration compared to that after 5 cycles, suggesting some CuO is reduced, which explains the activity recovery. For In/ACC, In 3*d* and O 1 *s* XPS spectra before reaction, after 5 cycles, and after regeneration with heating show little difference. However, the In 3*d* and O 1*s* spectra after regeneration with an applied potential do not have In^0 or In_2O_3 peaks but only $In(OH)_3$ peaks. The $In(OH)_3$ may result from leaching In^{3+} into solution (Figure S10), the generation of OH^- from HER near the cathode during regeneration, and subsequent precipitation of In^{3+} as $In(OH)_3$ on the cathode, thereby passivating this electrode. The differences in XPS results of electrodes regenerated by heating and an applied potential also highlight the importance of In or In_2O_3 as the active species for electrocatalytic NO_3^- reduction. However, it is not possible to further distinguish whether one or both species is primarily responsible for NO_3^- reduction activity because Indium is highly oxophilic, and this can cause In_2O_3 formation when exposed to the air prior to XPS analysis. Also, In_2O_3 can be reduced to In by an applied potential [52] during reactor operation.

3.6. Cost for ion exchange and (electro)catalytic treatment

In prior work, a cost comparison between IX and (electro)catalytic treatment using Pd as the benchmark catalyst was performed [43]. Here, we update the energy and catalyst metal costs for electrocatalytic treatment using our most favorable electrode, Cu 0.01 % Pd/ACC, and compare these to IX and catalytic treatment costs in details. Results are presented in Table 1, and all costs are expressed in 2023 dollars per 1000 gallons water treated. Note that costs presented for IX were mostly from pilot-scale studies [53,54] while costs for (electro)catalytic treatment were based on our bench-scale work. They have different implications on the actual costs for the full-scale application of these treatment technologies. With limited cost data in the literature, the goal of this work is to mitigate the gap of cost information for the electrocatalytic treatment, provide a conceptual level cost comparison and show promise of the electrocatalytic treatment, and promote further research and development of this emerging technology. For IX, capital costs are amortized over a 20-year period, and O&M costs include salt, brine disposal, and other such as labor, resin, and electricity. Two cost ranges are provided, and the lower range assumes the influent contains 1×MCL of NO_3^- and the upper range 2×MCL of NO_3^-. IX salt costs are comparable to capital costs. Disposal costs are highly variable depending on local options (i.e., sanitary sewer, on-site evaporation in ponds, and deep well injection), and vary from much less than to comparable to salt costs.

For catalytic NO_3^- treatment, a Pd–In/γ-Al_2O_3 catalyst is considered [10]. While other metals and supports have been explored in the literature, this catalyst has demonstrated by far the highest activity achieved by catalytic NO_3^- reduction in a continuous flow reactor. Hydrogen, Pd, and In costs are considered, and the first two dominate due to smaller amount and low cost of In relative to Pd [61,62]. The different Pd costs are provided assuming metal replacement after 20, 5, and 1 years. Hydrogen gas costs assume either steam methane reforming (least expensive) or electrochemical generation (most expensive), and are

Table 1
Cost of Ion Exchange (IX) and (Electro)Catalytic Treatment per 1000 Gallons Water Treated (Adapted with Permission from [43]. Copyright 2021 American Chemical Society.).

Ion Exchange (IX)[a]									
IX Salt O&M[b]		IX Disposal O&M[c]		IX Total O&M[d]	IX Capital[d]	IX Total[d]			
\$0.41, \$0.73		\$0.02–0.44		\$0.20–3.55 (\$1.17)	\$0.11–0.33 (\$0.20)	\$0.45–3.69 (\$1.42)			
				\$0.26–9.76 (\$2.05)	NA	\$0.52–9.91 (\$2.30)			
Catalytic Treatment[e]									
H_2 Gas[f]		Pd[g]		In[g]	Catalyst Total[g]				
\$0.06–0.14		\$0.07		\$$2.68\times10^{-5}$	\$0.13–0.22				
		\$0.27		\$$1.07\times10^{-4}$	\$0.33–0.41				
		\$1.33		\$$5.35\times10^{-4}$	\$1.39–1.47				
Electrocatalytic Treatment[h]									
Energy for Electrolysis[i]			Metal[j]			Ammonia Recovery[k]	Nafion Membrane[l]	Electrocatalytic Total	
Pd–In	Cu 0.01 % Pd		Pd–In		Cu 0.01 % Pd			Pd	Cu 0.01 % Pd
\$6.65	\$0.24		\$0.02		\$$1.95\times10^{-4}$	\$0.51	\$0.012	\$7.19	\$0.762
			\$0.09		\$$7.81\times10^{-4}$		\$0.04	\$7.29	\$0.791
			\$0.46		\$$3.90\times10^{-3}$		\$0.24	\$7.86	\$0.994

[a] All IX costs were in 2018 U.S. dollars in [43], and are converted to 6/2023 U.S. dollars using CPI inflation calculator from the U.S. Bureau of Labor Statistics website, https://www.bls.gov/data/inflation_calculator.htm.

[b] Lower cost is for Vale, OR from [53]. Higher cost is for Fruitland, ID from [54].

[c] From [55]. Values represent a range of costs for discharge to sanitary sewer, on-site evaporation in ponds, and deep well injection.

[d] From [56]. Based on USEPA cost estimating procedures for 0.17–1.09 MGD water treatment plant. Total O&M costs include salt and disposal. Lower range of costs is for treating 1×MCL of nitrate, and upper range of costs is for treating 2×MCL of nitrate. Capital costs were only reported for treating 1×MCL of nitrate. Values in the parenthesis are the averages.

[e] All catalytic costs were in 2018 U.S. dollars in the [43], and are converted to 6/2023 U.S. dollars using CPI inflation calculator from the U.S. Bureau of Labor Statistics website, https://www.bls.gov/data/inflation_calculator.htm. Pd and In costs are highly variable and are based on the 1/31/2023 spot price from https://tradingeconomics.com/ for Pd, and from https://www.dailymetalprice.com/ for In. Hydrogen, Pd and In costs are considered in the totals. All other costs are ignored.

[f] From [57]. Represents range of prices from steam methane reforming (least expensive) to reformer-electrolyzer-purifier technology, and to proton exchange membrane (most expensive).

[g] Values reflect Pd and In replacement times of 20 years, 5 years, and 1 year, respectively. Pd costs are based on nitrate reduction activities in a trickle-bed reactor from [10].

[h] All electrocatalytic costs are in 6/2023 U.S. dollars. Pd, Cu and In costs are highly variable and are based on the 1/31/2023 spot price from https://tradingeconomics.com/ for Pd and Cu, and from https://www.dailymetalprice.com/ for In.

[i] Based on the calculated energy consumptions using the filterpress flow reactor and ACC electrodes with different catalyst metals, and average cost (6 cents per kWh) of electricity for industry from Austin, TX in fiscal year 2018 [58]. The 2018 rate is chosen because there is an unusual increase in energy rate in 2019 and more recent data is unavailable. The energy consumption was calculated based on the average measured full cell potential, total electric charges passing through the flow reactor and the amount of nitrate removed using each electrode in a typical 2 h experiment in this work. The Faradaic efficiency is implied in the calculation. The full cell potentials for Pd–In/ACC and Cu 0.01 % Pd/ACC are –3.0 V and –2.0 V, respectively.

[j] Values reflect electrode replacement times of 20 years, 5 years, and 1 year, respectively. Metal costs include Pd and In costs, approximately equal to Pd costs due to a lower In loading and unit cost, and are based on electrocatalytic nitrate reduction activities measured in this work.

[k] From [59]. Costs were in 2017 Euros, and are converted to 6/2023 U.S. dollars first using https://www.inflationtool.com/ for inflation adjustment in Euros and then the EUR-to-USD exchange rate as of 6/30/2023 from https://www.wsj.com/market-data/quotes/fx/EURUSD/historical-prices for currency conversion. The cost represents the highest unit cost for ammonia recovery via stripping and acid adsorption because of the low nitrate concentration assumed in this cost analysis. The cost includes CAPEX, OPEX and deducts the value of ammonium sulfate produced.

[l] From [60], the unit cost for Nafion 117 membrane is estimated to be \$1733 per m^2 assuming in 2015 U.S. dollars based on the publication year of the paper, and \$2236 per m^2 in 06/2023 U.S. dollars converted using CPI inflation calculator from the U.S. Bureau of Labor Statistics website, https://www.bls.gov/data/inflation_calculator.htm. The conversion of the unit cost to the cost per 1000 gallons water treated assumes linearly scale up the area of the benchtop filterpress flow reactor based on the flow rate from 40 mL min^{-1} to 1 gallon per minute. The benchtop filterpress flow reactor used a piece of Nafion 117 membrane of 6 cm^2. The replacement time of the membrane is assumed 20 years, 5 years, and 1 year.

determined from the literature [57]. H_2 gas costs only dominate when Pd catalysts are replaced after 20 years of operation. In other cases, when Pd is replaced more frequently, Pd metal costs are dominant.

For electrocatalytic treatment, we consider both Pd–In/ACC and the optimal catalyst identified in this work, Cu 0.01 % Pd/ACC. The Pd–In /ACC is included for direct comparison to catalytic treatment where a Pd–In catalyst is used. The energy cost using Pd–In/ACC electrode is high mainly due to the low Faradaic efficiency (~3 %) with this catalyst. The energy cost for Cu 0.01 % Pd/ACC is much lower, at only \$0.24 per 1000 gallons water treated. This is due to the high Faradaic efficiency and low operating potential with this catalyst. As a result, total electrocatalytic costs for the Cu 0.01 % Pd/ACC are much lower than those for Pd–In/ACC.

Comparing the three technologies, costs for catalytic and electrocatalytic treatment are generally comparable to or lower than IX. The high O&M cost makes IX less attractive than catalytic and electrocatalytic treatment. In catalytic treatment, the total costs are dependent on Pd life span. While a 20-year catalyst life span is economically favorable, a more frequent (<1 year) catalyst replacement is likely due to irreversible fouling and metal attrition. The main barriers to lowering this cost are more efficient catalyst regeneration methods and improved reactor designs that minimize mass transfer limitations and improve overall activity. However, these presently remain unresolved challenges. The most promising is electrocatalytic treatment. This technology removes the primary barrier of using expensive precious metals in catalytic treatment by largely replacing it with an earth-abundant metal (i.e., Cu). The metal costs for Cu 0.01 % Pd/ACC are two orders of magnitude lower than Pd–In/ACC, and up to three orders of magnitude lower than conventional catalytic treatment. Recovering ammonia from the treated water can be optional. The costs for ammonia recovery through air stripping and acid scrubbing (including capital and O&M costs) can dominate the total costs for electrocatalytic treatment using Cu 0.01 % Pd/ACC but not when using Pd–In/ACC electrodes due to the higher costs of the latter. Nafion membrane is a significant cost only if it is replaced every year. The final costs for electrocatalytic treatment using Cu 0.01 % Pd/ACC, even with ammonia recovery, are competitive or outcompete other technologies under most scenarios suggesting the technology is economically viable.

CRediT authorship contribution statement

Charles J. Werth: Writing – review & editing, Resources, Project administration, Methodology, Investigation, Funding acquisition, Formal analysis, Data curation, Conceptualization. **Kuan-Lin Lee:** Methodology, Formal analysis. **Chenxu Yan:** Writing – review & editing, Writing – original draft, Validation, Methodology, Investigation, Formal analysis, Conceptualization. **Carolyn E. Brady:** Methodology, Investigation, Formal analysis. **Jacob P. Troutman:** Methodology, Investigation, Formal analysis. **Simon M. Humphrey:** Writing – review & editing, Methodology, Funding acquisition. **Syed Mubeen:** Writing – review & editing, Investigation, Funding acquisition, Formal analysis. **David M. Cwiertny:** Writing – review & editing, Methodology, Investigation, Funding acquisition.

Declaration of Competing Interest

The authors declare that they have no known competing financial interests or personal relationships that could have appeared to influence the work reported in this paper.

Data Availability

Data will be made available on request.

Acknowledgment

This work is supported by the Environmental Engineering program of the National Science Foundation (NSF) under the award numbers CBET-1922504 and by the Process Systems, Reaction Engineering and Molecular Thermodynamics program of the NSF under the award numbers CBET-1706797 and 1705255. We thank Michelle Mikesh from the Center for Biomedical Research Support (CBRS) Microscopy and Imaging Facility at the University of Texas at Austin (UT Austin) for the assistance of taking LR-TEM images. We thank Dr. Hugo Celio from the Texas Materials Institute (TMI) at UT Austin for collecting XPS spectra. We also thank Dr. Vincent Lynch from the Department of Chemistry and Faulkner Nanoscience and Technology Center at UT Austin for the assistance of PXRD pattern collection and analysis.

Appendix A. Supporting information

Supplementary data associated with this article can be found in the online version at doi:10.1016/j.apcatb.2024.124278.

References

[1] N.M. Dubrovsky, K.R. Burow, G.M. Clark, J.A.M. Gronberg, P.A. Hamilton, K.J. Hitt, D.K. Mueller, M.D. Munn, B.T. Nolan, L.J. Puckett, M.G. Rupert, T.M. Short, N.E. Spahr, L.A. Sprague, W.G. Wilber, The Quality of Our Nation's Waters−Nutrients in the Nation's Streams and Groundwater, 1992–2004: U.S. Geological Survey Circular 1350, U.S. Geological Survey, 2010. 〈https://water.usgs.gov/nawqa/nutrients/pubs/circ1350/〉 (accessed May 5, 2020).
[2] R.F. Spalding, M.E. Exner, Occurrence of nitrate in groundwater−a review, J. Environ. Qual. 22 (1993) 392–402, https://doi.org/10.2134/jeq1993.00472425002200030002x.
[3] B.T. Nolan, J.D. Stoner, Nutrients in groundwaters of the conterminous United States, 1992−1995, Environ. Sci. Technol. 34 (2000) 1156–1165, https://doi.org/10.1021/es9907663.
[4] K.R. Burow, B.T. Nolan, M.G. Rupert, N.M. Dubrovsky, Nitrate in groundwater of the United States, 1991−2003, Environ. Sci. Technol. 44 (2010) 4988–4997, https://doi.org/10.1021/es100546y.
[5] International Agency for Research on Cancer, World Health Organization, List of Classifications – IARC Monographs on the Identification of Carcinogenic Hazards to Humans, (2021). 〈https://monographs.iarc.who.int/list-of-classifications〉 (accessed October 7, 2021).
[6] National Primary Drinking Water Regulations Complete Table, U.S. Environmental Protection Agency, 2009. 〈https://www.epa.gov/sites/production/files/2016-06/documents/npwdr_complete_table.pdf〉.
[7] A. Kapoor, T. Viraraghavan, Nitrate removal from drinking water—review, J. Environ. Eng. 123 (1997) 371–380, https://doi.org/10.1061/(ASCE)0733-9372(1997)123:4(371).
[8] A. Zhu, P.D. Christofides, Y. Cohen, Energy consumption optimization of RO membrane desalination subject to feed salinity fluctuation, IFAC Proc. Vol. 42 (2009) 255–260, https://doi.org/10.3182/20090712-4-TR-2008.00039.
[9] A.M. Bergquist, M. Bertoch, G. Gildert, T.J. Strathmann, C.J. Werth, Catalytic denitrification in a trickle bed reactor: ion exchange waste brine treatment, J. Am. Water Works Assoc. 109 (2017) E129–E151, https://doi.org/10.5942/jawwa.2017.109.0055.
[10] M. Bertoch, A.M. Bergquist, G. Gildert, T.J. Strathmann, C.J. Werth, Catalytic nitrate removal in a trickle bed reactor: direct drinking water treatment, J. Am. Water Works Assoc. 109 (2017) E144–E171, https://doi.org/10.5942/jawwa.2017.109.0056.
[11] A.C.A. de Vooys, R.A. van Santen, J.A.R. van Veen, Electrocatalytic reduction of NO3− on palladium/copper electrodes, J. Mol. Catal. A Chem. 154 (2000) 203–215, https://doi.org/10.1016/S1381-1169(99)00375-1.
[12] M.A. Hasnat, S. Ben Aoun, M.M. Rahman, A.M. Asiri, N. Mohamed, Lean Cu-immobilized Pt and Pd films/–H+ conducting membrane assemblies: relative electrocatalytic nitrate reduction activities, J. Ind. Eng. Chem. 28 (2015) 131–137, https://doi.org/10.1016/j.jiec.2015.02.008.
[13] O.A. Petrii, Y.A. Akbaeva, T.Y. Safonova, V.S. Kondrasheva, E.N. Kolosov, G. A. Tsirlina, V.M. Gryaznov, Intensification of the nitrate anion reduction on a membrane palladium electrode, Russ. J. Electrochem. 38 (2002) 220–223, https://doi.org/10.1023/A:1016884718990.
[14] J.F.E. Gootzen, P.G.J.M. Peeters, J.M.B. Dukers, L. Lefferts, W. Visscher, J.A.R. van Veen, The electrocatalytic reduction of NO3− on Pt, Pd and Pt + Pd electrodes activated with Ge, J. Electroanal. Chem. 434 (1997) 171–183, https://doi.org/10.1016/S0022-0728(97)00093-4.
[15] T.Ya Safonova, O.A. Petrii, Effect of inorganic cations on the electroreduction of nitrate anions on Pt|Pt electrodes in sulfuric acid solutions, J. Electroanal. Chem. 448 (1998) 211–216, https://doi.org/10.1016/S0022-0728(97)00110-1.
[16] M. Duca, V. Kavvadia, P. Rodriguez, S.C.S. Lai, T. Hoogenboom, M.T.M. Koper, New insights into the mechanism of nitrite reduction on a platinum electrode, J. Electroanal. Chem. 649 (2010) 59–68, https://doi.org/10.1016/j.jelechem.2010.01.019.
[17] O. Brylev, M. Sarrazin, L. Roué, D. Bélanger, Nitrate and nitrite electrocatalytic reduction on Rh-modified pyrolytic graphite electrodes, Electrochim. Acta 52 (2007) 6237–6247, https://doi.org/10.1016/j.electacta.2007.03.072.
[18] O. Brylev, M. Sarrazin, D. Bélanger, L. Roué, Rhodium deposits on pyrolytic graphite substrate: physico-chemical properties and electrocatalytic activity towards nitrate reduction in neutral medium, Appl. Catal. B Environ. 64 (2006) 243–253, https://doi.org/10.1016/j.apcatb.2005.11.016.
[19] M.C.P.M. da Cunha, J.P.I. De Souza, F.C. Nart, Reaction pathways for reduction of nitrate ions on platinum, rhodium, and platinum−rhodium alloy electrodes, Langmuir 16 (2000) 771–777, https://doi.org/10.1021/la990638s.
[20] D. De, E.E. Kalu, P.P. Tarjan, J.D. Englehardt, Kinetic studies of the electrochemical treatment of nitrate and nitrite ions on Iridium-modified carbon fiber electrodes, Chem. Eng. Technol. 27 (2004) 56–64, https://doi.org/10.1002/ceat.200401832.
[21] G.E. Dima, A.C.A. de Vooys, M.T.M. Koper, Electrocatalytic reduction of nitrate at low concentration on coinage and transition-metal electrodes in acid solutions, J. Electroanal. Chem. (2003) 15–23, https://doi.org/10.1016/S0022-0728(02)01443-2.
[22] O. Ghodbane, M. Sarrazin, L. Roué, D. Bélanger, Electrochemical reduction of nitrate on pyrolytic graphite-supported Cu and Pd–Cu electrocatalysts, J. Electrochem. Soc. 155 (2008) F117, https://doi.org/10.1149/1.2900094.
[23] M.A. Hasnat, I. Ishibashi, K. Sato, R. Agui, T. Yamaguchi, K. Ikeue, M. Machida, Electrocatalytic reduction of nitrate using Cu–Pd and Cu–Pt cathodes/H+-conducting solid polymer electrolyte membrane assemblies, BCSJ 81 (2008) 1675–1680, https://doi.org/10.1246/bcsj.81.1675.
[24] I. Katsounaros, D. Ipsakis, C. Polatides, G. Kyriacou, Efficient electrochemical reduction of nitrate to nitrogen on tin cathode at very high cathodic potentials, Electrochim. Acta 52 (2006) 1329–1338, https://doi.org/10.1016/j.electacta.2006.07.034.
[25] Y. Wang, J. Qu, R. Wu, P. Lei, The electrocatalytic reduction of nitrate in water on Pd/Sn-modified activated carbon fiber electrode, Water Res. 40 (2006) 1224–1232, https://doi.org/10.1016/j.watres.2006.01.017.
[26] P. Gayen, J. Spataro, S. Avasarala, A.-M. Ali, J.M. Cerrato, B.P. Chaplin, Electrocatalytic reduction of nitrate using Magnéli phase TiO2 reactive electrochemical membranes doped with Pd-based catalysts, Environ. Sci. Technol. 52 (2018) 9370–9379, https://doi.org/10.1021/acs.est.8b03038.
[27] S. Garcia-Segura, M. Lanzarini-Lopes, K. Hristovski, Paul Westerhoff, Electrocatalytic reduction of nitrate: fundamentals to full-scale water treatment applications, Appl. Catal. B Environ. 236 (2018) 546–568, https://doi.org/10.1016/j.apcatb.2018.05.041.
[28] J.-X. Liu, D. Richards, N. Singh, B.R. Goldsmith, Activity and selectivity trends in electrocatalytic nitrate reduction on transition metals, ACS Catal. 9 (2019) 7052–7064, https://doi.org/10.1021/acscatal.9b02179.
[29] D. Anastasiadou, Y. van Beek, E.J.M. Hensen, M. Costa Figueiredo, Ammonia electrocatalytic synthesis from nitrate (n/a), Electrochem. Sci. Adv. (2021) e2100220, https://doi.org/10.1002/elsa.202100220.

[30] C. Yan, S. Kakuturu, A. Butzlaff, D. Cwiertny, S. Mubeen, C. Werth, Scalable reactor design for electrocatalytic nitrite reduction with minimal mass transfer limitations, ACS EST Engg. 1 (2021) 204–215, https://doi.org/10.1021/acsestengg.0c00054.
[31] K.P. Kepp, A quantitative scale of oxophilicity and thiophilicity, Inorg. Chem. 55 (2016) 9461–9470, https://doi.org/10.1021/acs.inorgchem.6b01702.
[32] F.C. Walsh, C. Ponce de León, Progress in electrochemical flow reactors for laboratory and pilot scale processing, Electrochim. Acta 280 (2018) 121–148, https://doi.org/10.1016/j.electacta.2018.05.027.
[33] T. Kumar, N. Xavier, M. Ramya, A high-performance liquid chromatography method for determination of genotoxic impurity hydroxylamine in drug substances, J. Chromatogr. Sci. 57 (2019) 63–70, https://doi.org/10.1093/chromsci/bmy082.
[34] Y. Liao, A. Li, Indium hydride generation atomic absorption spectrometry with in situ preconcentration in a graphite furnace coated with palladium, J. Anal. Spectrom. 8 (1993) 633–636, https://doi.org/10.1039/JA9930800633.
[35] B.P. Chaplin, J.R. Shapley, C.J. Werth, Regeneration of sulfur-fouled bimetallic Pd-based catalysts, Environ. Sci. Technol. 41 (2007) 5491–5497, https://doi.org/10.1021/es0704333.
[36] D.P. Durkin, T. Ye, J. Choi, K.J.T. Livi, H.C.D. Long, P.C. Trulove, D.H. Fairbrother, L.M. Haverhals, D. Shuai, Sustainable and scalable natural fiber welded palladium-indium catalysts for nitrate reduction, Appl. Catal. B Environ. 221 (2018) 290–301, https://doi.org/10.1016/j.apcatb.2017.09.029.
[37] S. Guo, K. Heck, S. Kasiraju, H. Qian, Z. Zhao, L.C. Grabow, J.T. Miller, M.S. Wong, Insights into nitrate reduction over indium-decorated Palladium nanoparticle catalysts, ACS Catal. 8 (2018) 503–515, https://doi.org/10.1021/acscatal.7b01371.
[38] S. Xu, Y. Shi, Z. Wen, X. Liu, Y. Zhu, G. Liu, H. Gao, L. Sun, F. Li, Polystyrene spheres-templated mesoporous carbonous frameworks implanted with cobalt nanoparticles for highly efficient electrochemical nitrate reduction to ammonia, Appl. Catal. B Environ. 323 (2023) 122192, https://doi.org/10.1016/j.apcatb.2022.122192.
[39] Z. Niu, S. Fan, X. Li, Z. Liu, J. Wang, J. Duan, M.O. Tadé, S. Liu, Facile Tailoring of the electronic structure and the d-band center of copper-doped cobaltate for efficient nitrate electrochemical hydrogenation, ACS Appl. Mater. Interfaces (2022), https://doi.org/10.1021/acsami.2c04789.
[40] X. Xu, L. Hu, Z. Li, L. Xie, S. Sun, L. Zhang, J. Li, Y. Luo, X. Yan, M.S. Hamdy, Q. Kong, X. Sun, Q. Liu, Oxygen vacancies in Co3O4 nanoarrays promote nitrate electroreduction for ammonia synthesis, Sustain. Energy Fuels (2022), https://doi.org/10.1039/D2SE00830K.
[41] J. Li, G. Zhan, J. Yang, F. Quan, C. Mao, Y. Liu, B. Wang, F. Lei, L. Li, A.W.M. Chan, L. Xu, Y. Shi, Y. Du, W. Hao, P.K. Wong, J. Wang, S.-X. Dou, L. Zhang, J.C. Yu, Efficient ammonia electrosynthesis from nitrate on strained Ruthenium nanoclusters, J. Am. Chem. Soc. 142 (2020) 7036–7046, https://doi.org/10.1021/jacs.0c00418.
[42] B.P. Chaplin, M. Reinhard, W.F. Schneider, C. Schüth, J.R. Shapley, T. J. Strathmann, C.J. Werth, Critical review of Pd-Based catalytic treatment of priority contaminants in water, Environ. Sci. Technol. 46 (2012) 3655–3670, https://doi.org/10.1021/es204087q.
[43] C.J. Werth, C. Yan, J.P. Troutman, Factors impeding replacement of ion exchange with (electro)catalytic treatment for nitrate removal from drinking water, ACS EST Engg. 1 (2021) 6–20, https://doi.org/10.1021/acsestengg.0c00076.
[44] R. Abdallah, F. Geneste, T. Labasque, H. Djelal, F. Fourcade, A. Amrane, S. Taha, D. Floner, Selective and quantitative nitrate electroreduction to ammonium using a porous copper electrode in an electrochemical flow cell, J. Electroanal. Chem. 727 (2014) 148–153, https://doi.org/10.1016/j.jelechem.2014.06.016.
[45] M. Machida, K. Sato, I. Ishibashi, M.A. Hasnat, K. Ikeue, Electrocatalytic nitrate hydrogenation over an H+-conducting solid polymer electrolyte membrane–modified cathode assembly, Chem. Commun. (2006) 732–734, https://doi.org/10.1039/B514155A.
[46] K.S. Rajmohan, R. Chetty, Enhanced nitrate reduction with copper phthalocyanine-coated carbon nanotubes in a solid polymer electrolyte reactor, J. Appl. Electrochem. 47 (2017) 63–74, https://doi.org/10.1007/s10800-016-1020-7.
[47] D. Reyter, D. Bélanger, L. Roué, Optimization of the cathode material for nitrate removal by a paired electrolysis process, J. Hazard. Mater. 192 (2011) 507–513, https://doi.org/10.1016/j.jhazmat.2011.05.054.
[48] L. Szpyrkowicz, S. Daniele, M. Radaelli, S. Specchia, Removal of NO3− from water by electrochemical reduction in different reactor configurations, Appl. Catal. B Environ. 66 (2006) 40–50, https://doi.org/10.1016/j.apcatb.2006.02.020.
[49] K.W. Goh, M.R. Johan, Y.H. Wong, Enhanced structural properties of In2O3 nanoparticles at lower calcination temperature synthesised by co-precipitation method, Micro Nano Lett. 13 (2018) 270–275, https://doi.org/10.1049/mnl.2017.0540.
[50] M.C. Biesinger, Advanced analysis of copper X-ray photoelectron spectra, Surf. Interface Anal. 49 (2017) 1325–1334, https://doi.org/10.1002/sia.6239.
[51] M.C. Biesinger, L.W.M. Lau, A.R. Gerson, R.St.C. Smart, Resolving surface chemical states in XPS analysis of first row transition metals, oxides and hydroxides: Sc, Ti, V, Cu and Zn, Appl. Surf. Sci. 257 (2010) 887–898, https://doi.org/10.1016/j.apsusc.2010.07.086.
[52] Y. Liang, W. Zhou, Y. Shi, C. Liu, B. Zhang, Unveiling in situ evolved In/In2O3−x heterostructure as the active phase of In2O3 toward efficient electroreduction of CO2 to formate, Sci. Bull. 65 (2020) 1547–1554, https://doi.org/10.1016/j.scib.2020.04.022.
[53] L. Wang, A.S.C. Chen, A. Wang, W.E. Condit, Arsenic and Nitrate Removal from Drinking Water by Ion Exchange U.S. EPA Demonstration Project at Vale, OR – Final Performance Evaluation Report, U.S. Environmental Protection Agency, Washington, D.C., 2011. https://nepis.epa.gov/Exe/ZyPDF.cgi/P100AVF2.PDF?Dockey=P100AVF2.PDF.
[54] L. Wang, A.S.C. Chen, N. Tong, C.T. Coonfare, Arsenic Removal from Drinking Water by Ion Exchange U.S. EPA Demonstration Project at Fruitland, ID – Six-Month Evaluation Report, U.S. Environmental Protection Agency, Washington, D. C., 2007. ⟨http://www.epa.gov/nrmrl/pubs/600r07017/600r07017.pdf⟩.
[55] V.B. Jensen, J.L. Darby, Brine disposal options for small systems in California's central valley, J. AWWA 108 (2016) E276–E289, https://doi.org/10.5942/jawwa.2016.108.0045.
[56] V.B. Jensen, J.L. Darby, C. Seidel, C. Gorman, Drinking Water Treatment for Nitrate, Center for Watershed Sciences, University of California, Davis, Davis, California, 2012. ⟨http://groundwaternitrate.ucdavis.edu/files/139107.pdf⟩.
[57] P. Nikolaidis, A. Poullikkas, A comparative overview of hydrogen production processes, Renew. Sustain. Energy Rev. 67 (2017) 597–611, https://doi.org/10.1016/j.rser.2016.09.044.
[58] Austin Energy, Austin Energy Rates - Cents Per Kilowatt Hour by Customer Class: Austin Energy Rates - Cents Per Kilowatt Hour by Customer Class, (2021). https://doi.org/10.26000/040.000010 (accessed February 2, 2023).
[59] H.W.H. Menkveld, E. Broeders, Recovery of ammonium from digestate as fertilizer, Water Pract. Technol. 12 (2017) 514–519, https://doi.org/10.2166/wpt.2017.049.
[60] G. Hernández-Flores, H.M. Poggi-Varaldo, O. Solorza-Feria, M.T. Ponce-Noyola, T. Romero-Castañón, N. Rinderknecht-Seijas, J. Galíndez-Mayer, Characteristics of a single chamber microbial fuel cell equipped with a low cost membrane, Int. J. Hydrog. Energy 40 (2015) 17380–17387, https://doi.org/10.1016/j.ijhydene.2015.10.024.
[61] J.K. Choe, A.M. Bergquist, S. Jeong, J.S. Guest, C.J. Werth, T.J. Strathmann, Performance and life cycle environmental benefits of recycling spent ion exchange brines by catalytic treatment of nitrate, Water Res. 80 (2015) 267–280, https://doi.org/10.1016/j.watres.2015.05.007.
[62] J.K. Choe, M.H. Mehnert, J.S. Guest, T.J. Strathmann, C.J. Werth, Comparative assessment of the environmental sustainability of existing and emerging perchlorate treatment technologies for drinking water, Environ. Sci. Technol. 47 (2013) 4644–4652, https://doi.org/10.1021/es3042862.